Swift heavy ion irradiation effect on structural, morphological and mechanical properties of Zr 70 Ni 30 metallic glass

Wafa Boukhemkhem, Mahmoud Izerrouken, Matteo Ghidelli, Thomas Pardoen, Ali Sari, Abdel Yazid Khereddine, Ali Meftah

Swift heavy ion irradiation induced defects in $Zr_{70}Ni_{30}$ metallic glass

W. Boukhemkhem[a], M. Izerrouken[b], M. Ghidelli[c], T. Pardoen[d], A. Sari[e], A. Kheireddine[f] and A.Meftah[a]

[a]*LRPCSI, Faculty of Sciences, Université 20 Août 1955-Skikda, 21000 Skikda, Algeria.*

[b]*Nuclear Research Center of Draria, BP 43, Sebbala, Draria, Algiers, Algeria*

[c]*Laboratoire des Sciences des Procédés et des Matériaux (LSPM), CNRS, Université Sorbonne Paris Nord, 93430, Villetaneuse, France*

[d]*Institute of Mechanics, Materials and Civil Engineering, UCLouvain, Place Sainte-Barbe 2, 1348 Louvain-la-Neuve, Belgium*

[e]*Nuclear Research Center of Birine, BP 108, Ain-Oussera, Djelfa, Algeria*

[f]*Center for Development of Advanced Technologies, Algiers, Algeria*

Corresponding author: M. Izerrouken

Email: izerrouken@yahoo.com

m-izerrouken@crnd.dz

Swift heavy ion irradiation induced defects in $Zr_{70}Ni_{30}$ metallic glass

Metallic glass films are considered more and more in the nuclear field for different coating applications owing to the advantageous performances but the response to irradiation remains to be properly investigated. $Zr_{70}Ni_{30}$ metallic glass films were irradiated by 0.71 MeV/u $^{129}Xe^{+23}$ ions in the fluence range 5×10^{12} to 8×10^{13} ions/cm^2. After ion irradiation, the structural, morphological, and mechanical properties were determined using grazing incidence X-ray diffraction (GI-XRD), atomic force microscopy (AFM), and nanoindentation for the as-deposited and irradiated samples. Interestingly, the Xe ion-induced surface smooth when the ions fluence is set to 1×10^{13} Xe/cm^2. One-dimensional power spectral density of the AFM data of irradiated film demonstrated that the irradiation-induced evolution of the surface morphology can be attributed to a transition between viscous flow and the evaporation-condensation mechanism. The amorphous structure was unaffected after irradiation up to a fluence of 8×10^{13} ions/cm^2. Nanoindentation revealed first a softening as the fluence increases up to 4×10^{13} ions/cm^2, reflecting the creation of free volume defects. While the hardness and Young's modulus slightly increasing when reaching 8×10^{13} ions/cm^2. Moreover, at a critical dose of 109 dpa, the hardness is found to increase. We show by the inelastic thermal spike model that the metallic glass's overall performance also reveals the track's formation with a radius of 7 nm under ion irradiation.

Keywords: $Zr_{70}Ni_{30}$ metallic glass; ion irradiation; structural evolution; thermal spike model.

1. Introduction

Zirconium alloys constitute one of the most attractive and convenient materials for cladding applications in nuclear reactors owing to the low thermal neutron capture cross-section and adequate mechanical performances [**1**,**2**]. In contrast to the conventional crystalline Zr-alloys, amorphous alloys or metallic glasses (MGs) counterparts with diverse compositions were processed through exploiting their high

glass-forming ability [**3**,**4**]. MGs show a liquid-like atomic configuration and the absence of crystalline defects such as grain boundaries and dislocations [**5**,**6**]. This confers interesting mechanical and chemical properties such as high strength (2-3 GPa), high elastic limit (~2 %), good fracture toughness (40-50 $MPa.m^{1/2}$), and excellent resistance to corrosion [**4**,**6**]. Thin-film metallic glasses (TFMGs) can be prepared using different kinds of methods, such as physical vapor deposition (PVD), including evaporation and sputtering [**7**,**8**] and pulsed laser deposition [**9**], showing fascinating mechanical size effects boosting mechanical properties beyond those of bulk counterparts [**10**]. For instance, Jiang et al. [**11**] found a high elastic strain limit of about 6.6% for the $Ni_{60}Nb_{40}$ metallic glass films. Jang et al. [**12**] also observed that the 100 nm Zr-based MG has an outstanding combination of high strength (~2.25GPa) and increased ductility (~25%).

In addition, Zr-based MGs have very high thermal stability with an exceptionally wide super cooled liquid region reaching [**3**,**13**] enabling large stability of the glass phase. For these reasons, Zr-based MGs appear as a class of promising candidates in nuclear irradiation environments [**14**,**15**] due to the unique combination of large mechanical properties, thermodynamic stability and the absence of crystalline defects providing a high irradiation resistance, unlike their crystalline counterparts [**16**,**17**]. Li et al. [**16**] reported that helium irradiation induced more severe peelings on the surface of the crystalline material $Zr_{67}Ni_{33}$ than the $Zr_{47.9}Ti_{0.3}Cu_{39.3}Ni_{3.1}Al_{9.4}$ bulk MG, which shows the formation of tiny bubbles of Helium. On the other hand, according to Wang et al. [**17**], in the case of 500 keV helium irradiated polycrystalline tungsten (W) at a fluence of 1×10^{18} ion/cm^2, the high-stress concentration at bubbles helium precipitated at grain boundaries causes delamination and peeling, whereas no obvious damage was observed in the $Zr_{64}Cu_{17.8}Ni_{10.7}Al_{7.5}$ bulk MG.

Despite these promising results, few and controversial studies still deal with understanding the structural/mechanical evolution of MGs during irradiation through different categories of radiation (charged particles, neutrons and gamma rays). As an example, irradiation by electrons [**18**–**20**] and by ions [**21**,**22**] induces the crystallization of Zr-based MGs ribbons as well as bulk systems [**15**,**23**]. Irradiation-induced crystallization was investigated by Nagase et al. [**24**] who proposed three mechanisms to explain this phenomenon: the first one is the increase of free energy of the system, which reaches a threshold value due to the formation of radiation defects such as free volume and anti-free volume inside the amorphous solid. The second one is the random formation of a crystalline cluster near the radiation defects due to a reduction of the local strain, while the facilitated atomic diffusion represents the third one due to the damage caused by irradiation promoting crystallization. Other results, in contrast, indicated that Zr bulk MGs remain amorphous under high energy ion irradiation (E>1MeV) [**14**,**25**,**26**]. Different studies reported that ion irradiation induces variations of free volume [**27**,**28**], of interatomic distances [**15**,**29**], and some structural relaxation [**30**] in the Zr-based MGs. The collapse of short-range order (SRO) has been further reported by Qiu et al. [**31**] in $Ni_{50}Nb_{10}Zr_{15}Ti_{15}Pt_{7.5}Cu_{2.5}$ MG ribbon irradiated with 3 MeV Au^{2+} ions at a fluence of 1×10^{14} ions/cm^2. Moreover, the mechanical properties were modified after ion irradiation [**15**,**23**]. Iqbal et al. [**23**] found that hardness and elastic modulus increase by 43% and 25%, respectively. Similar results were also reported by Luo et al. [**15**] for $Zr_{61.5}Cu_{21.5}Fe_5Al_{12}$ bulk MG irradiated by 300 keV Ar^+ ions due to the precipitation of nanoparticles with a face-centered cubic (fcc) structure and a size of 5 nm.

In this paper, we investigate the ion irradiation damage of Zr-Ni thin-film metallic glasses. This composition was selected owing to the high stability at room temperature

together with a large region of amorphization, from 10 up to 80 at % of Zr [**32**,**33**]. To our knowledge, only Nagase et al. [**19**,**20**] and Tyagi and colleagues [**34**,**35**] investigated the effect of radiation damage on the binary (Zr-Ni) MGs, in particular for the compositions $Zr_{66.6}Ni_{33.3}$ and $Zr_{67}Ni_{33}$. The present work is mainly focused on the impact of swift heavy ion irradiation, where the electronic energy loss is dominant, on the structural, morphological and mechanical properties of the binary $Zr_{70}Ni_{30}$ thin film metallic glass by using several techniques. The goal is to characterize the micro-structured surface evolution as well as mechanical behavior under ion irradiation, understand the underlying mechanisms, and, consequently, to determine its potential applications as coatings for nuclear reactor components. In addition, inelastic thermal spike [**36**] calculations are performed to further highlight the impact of electronic energy loss and investigate latent track formation in $Zr_{70}Ni_{30}$ metallic glass.

2. Experimental procedures

Zr_xNi_{100-x} (x=70 at.%), thin-film metallic glasses (TFMGs) were prepared by DC-magnetron sputtering on a cleaned Si (100) substrate within a clean room (class 1000) to limit contamination [**10**,**37**].

After processing, the $Zr_{70}Ni_{30}$ films were irradiated with 0.71MeV/u $^{129}Xe^{23+}$ ions at room temperature to fluences of 5×10^{12}, 1×10^{13}, 2×10^{13}, 4×10^{13} and 8×10^{13} ions/cm^2. The irradiations were performed at GANIL, Caen, France, using the IRRSUD beam line. The samples were partially masked, enabling a direct comparison between the irradiated and the non-irradiated parts for each sample. The electronic stopping power S_e, nuclear stopping power S_n and projected ion range R_p deduced using the code SRIM 2008 (Stopping and Range of Ions in Matter) [**38**] are respectively equal to 23.29 keV/nm, 0.22 keV/nm and 7180 nm. The ion range is larger than the film thickness;

hence no Xe ion is implanted in the irradiated sample. The displacement per atom (dpa) corresponding to the irradiation fluences was calculated using equation (1) to characterize the irradiation damage [**39**]:

$$dpa = \frac{\phi\, N_d\, A}{\rho\; d\; N_A} \quad , \tag{1}$$

where ϕ is the Xenon ion fluence, N_d is the number of displacements per ion, A is the target material's molecular mass, ρ is the atomic density of $Zr_{70}Ni_{30}$, d is the penetration depth, and N_A is Avogadro's number. The displacement damage (N_d/d) was calculated using SRIM 2003 code with displacement energy of 40 eV for Zr and Ni atoms, respectively, and using the 'quick calculation of damage mode.' The total vacancy induced in the layer is 1454/ion leading to a total dose of 13.64, 27.28, 54.56, 109.12 and 218.24 dpa, respectively, for each fluence.

The radiation damage was then investigated using several techniques. The structural characterization was performed by grazing incidence X-ray diffraction (GI-XRD) using a Panalytical X'PERT-PRO MPD X-ray diffractometer with a Cu $K\alpha_1$ radiation (λ =1.5406 Å) and a PIXcel1D detector. The incident angle was optimized to be 1.6° to avoid the influence of the Si substrate on the collected data. The root-mean-square (RMS) roughness and surface topography of unirradiated and irradiated films were examined using atomic force microscopy (AFM) (type: MFP-3D from Asylum Research, an Oxford Instruments company) in contact mode, with a silicon probe of 9 nm tip radius. In addition, the Power Spectral Density (PSD) was then used to provide further information regarding the dominant mechanism responsible for RMS evolution versus fluence. The power spectral density of a surface is a mathematical tool that decomposes the surface into contributions of different spatial frequencies (wave

vectors) via Fourier analysis of the surface [**40**]. The one-dimensional PSD is calculated from the AFM images by the WSxM (Windows Scanning X Microscope) software [**41**]. Nanoindentation experiments were used to probe the mechanical properties. All measurements were carried out using a continuous stiffness measurement (CSM) mode with a Berkovich diamond indenter at room temperature. A maximum load of 3.5 mN and a loading time of 10 s were applied for each sample. In order to obtain accurate statistical data, different indents were performed on each sample with 0.15 mm spacing between each indent. The hardness (*H*) and Young's modulus (*E*) values were determined using the Oliver-Pharr method [**42**]. Additional analysis using a thermal spike model was also performed to check the effect of 0.71 MeV/u Xe ion irradiation on the formation of the ion track in $Zr_{70}Ni_{30}$.

3. Results and discussion

3.1. Characterization of the as-deposited $Zr_{70}Ni_{30}$ metallic glass

Figure 1(a) shows GI-XRD spectrum collected in the 2θ range of 20-80°. A broad halo is observed at 37°, confirming the amorphous structure of the $Zr_{70}Ni_{30}$ TFMG, which is according to that finding in previous works [**37**,**43**]. Figure 1(b) shows 2D and 3D AFM images over a 10 μm×10 μm of the $Zr_{70}Ni_{30}$ film, respectively. The RMS roughness of the surface is about 0.94±0.18nm and is rather consistent, with little hills (protrusions)-like morphology as indicated by white arrows.

Figure 1(c) shows the morphologies of the $Zr_{70}Ni_{30}$ TFMGs in a cross-section view. Observations have been carried out using a field-emission scanning electron microscope (FE-SEM) after cleavage of the Si substrate enabling propagation of a crack from the Si substrate to the films, see Refs. [**44**,**45**] for more details, Figure 1(c) reveals that the film thickness is uniform, with a variation of by only a few nm, as expected for sputtered

deposition [**44**]. The film thickness is about 1200 nm. The hardness (*H*) and Young's modulus (*E)* are respectively equal to 7.7±0.45 GPa and 105.8±11.3 GPa, similar to the values determined by Volland et al. [**46**].

3.2. Irradiation effects on the $Zr_{70}Ni_{30}$ metallic glass properties

3.2.1. Structural evolution

The GI-XRD patterns obtained before and after irradiation can be found in Figure 2. All patterns show a broad band without any sharp diffraction peaks. This indicates that ion irradiation up to a fluence of 8×10^{13} ions/cm^2 does not modify the structure of $Zr_{70}Ni_{30}$ TFMG, and that all samples are still amorphous. The maintained amorphous structure is in agreement with the results obtained on $Zr_{67}Ni_{33}$ MG irradiated by 100 keV He ion at a fluence lower than 6×10^{17} He/cm^2 [**34**,**35**]. On the other hand, the electron irradiation-induced crystallization was reported in the works conducted by Nagase et al. [**19**,**20**] on $Zr_{66.6}Ni_{33.3}$ amorphous alloy irradiated at room temperature with 2 MeV electrons for a flux between 1.6×10^{24} and 1.1×10^{25} e/m^2.s.

However, after fitting the results with a Lorentzian function, we did not observe any clear evolution of the band position and full width at half maximum (FWHM) of the band after ion irradiation in the investigated fluence range from 5×10^{12} to 8×10^{13} ions/cm^2. In the literature, Contradictory results show the band position shifting or remaining unchanged without any form of precipitation of crystals. For example, for $Zr_{50.7}Cu_{28}Ni_9Al_{12.3}$ MG irradiated with 7 MeV Xe^{26+} ions in the dose range (0.5 and 1 dpa), Bian et al. [**28**] found band position shifts towards a lower angle after irradiation, interpreted as an increase of the average inter-atomic spacing associated to an increase of free volume. Qiu et al. [**31**] found that for $Ni_{50}Nb_{10}Zr_{15}Ti_{15}Pt_{7.5}Cu_{2.5}$ MG ribbon irradiated by 3 MeVAu^{2+} ions, no apparent change in the broad peak position, they also

reported that at a low dose of 0.49 and 4.9 dpa the destruction of the short-range order (SRO) was occurred, which leads to an excess of free volume, with a further increase of the dose to 49 dpa, the free volume decreases which is attributed to the formation of a local structure caused by the enhancement of the atomic mobility.

3.2.2. Surface morphology evolution

The surface morphology after 0.71 MeV/u $^{129}Xe^{23+}$ ion irradiation at different fluences is shown in Figure 3. The small hills observed on the deposited sample disappear after ion irradiation, and the surface becomes smoother. This is further confirmed in Figure 4, with the root-mean-square (RMS) roughness evolution under different fluences. First, the RMS roughness decreases in the fluence range of 0 up to 1×10^{13} ions/cm^2 from 0.94±0.18 nm for unirradiated sample down to 0.19±0.01 nm for sample irradiated at 1×10^{13} ions/cm^2. Then, the RMS roughness increases slightly to 0.37±0.09 nm and 0.51±0.02 nm, respectively, at a fluence of 2×10^{13} ions/cm^2 and 4×10^{13} ions/cm^2. Finally, it remains approximately constant at higher fluence, up to 8×10^{13} ions/cm^2. According to the literature, ion irradiation has thus two main effects on the surface morphology of a solid: surface roughening and smoothening. The first is caused by the sputtering atoms, and the second is induced by material transport [**47**]. The above results agree with previous work [**48**] on amorphous Fe-Ni thin films irradiated with 103 MeV Au^{9+} ions. Several authors also reported that irradiation-induced smoothening and roughening phenomena depend on the material, particle energy, and fluence. For example, similar surface smoothening was reported in Refs. [**49**,**50**]. Moreover, surface roughening was found in other investigations [**51**,**52**] and attributed to the damage induced under ion irradiation in different metallic glasses.

The Power Spectral Density (PSD) is used to interpret the RMS evolution with irradiation fluence. This gives a representation of the surface roughness amplitude as a function of the spatial frequency of the roughness [**40**], which helps understand the mechanism responsible for smoothening and roughening the surface after ion irradiation. The PSD data (see Figure 5) show two distinct domains. One domain at a low spatial frequency (region I) corresponds to the uncorrelated white noise, and the second one at a high frequency (region II) represents correlated surface features [**48**,**53**]. Moreover, according to Tong and Williams study [**54**], at low spatial frequency values, a flat plateau extends out to the critical spatial frequency, after which the power spectral density decreases linearly due to surface smoothening. Four mechanisms were discussed; plastic flow, evaporation-condensation, bulk diffusion, and surface diffusion corresponding respectively to the slop values of 1, 2, 3 and 4 [**55**]. In our case, the fitting is performed in the linear region, which begins from the critical spatial frequency value ($0.045 nm^{-1}$). The obtained values of the slope of the linear fit are summarized in Table 1. When the fluence increases from 0 to 2×10^{13} ions/cm^2, the slope varies from 3 to 1. Thus, the surface morphology modification is interpreted as a combination between plastic flow and evaporation-condensation at low fluence ($\leq2\times10^{13}$ ions/cm^2). At higher fluence ($>2\times10^{13}$ ions/cm^2), the value is close to 2, which means that the evaporation-condensation process can explain the roughness increase at high fluence. The latter evolution is attributed to the temperature increase along the ion path as found using the thermal spike model addressed hereafter. A similar change of the roughness has been observed by Pookat et al. [**56**] in amorphous $Co_{77}Fe_{23}$ thin films irradiated with 100 MeV Ag^{7+}, where the smoothening of the surface topography is due to the viscous flow occurs at a fluence of 1×10^{11} ions/cm^2 and the evaporation-condensation

mechanism caused by the sputtering is already activated at a fluence of 1×10^{12} ions/cm^2 and 3×10^{13} ions/cm^2.

3.2.3. Mechanical properties

The load-depth response obtained during the nanoindentation experiments were used to extract the mechanical properties summarized in Table 2. Figure 6 provides the evolution of hardness (*H)* and Young's modulus (*E)* as a function of the fluence. Both (*H)* and (*E)* decrease with increasing fluence up to 4×10^{13} ions/cm^2 from 7.7±0.45 GPa down to 4.9±0.15 GPa and from 105.8±11.3 GPa down to 62.6±4.6 GPa, respectively. This is followed by a slight increase when then fluence grows up to 8×10^{13} ions/cm^2.

As well known, the Young's modulus of a material is inversely correlated with the distance to neighbor atoms, hence a decrease in the amount of the free volume tend to lead to an increase of the modulus [**57**]. Thus, the elastic modulus evolution reveals an irradiation-induced free volume enhancement (decrease of atomic density) up to a fluence of 4×10^{13}ions/cm^2, which means that the observed reduction in the stiffness and strength can be attributed to the damage induced by either free volume or nano-voids through ion-solid collision [**58**], which probably results in the softening of the $Zr_{70}Ni_{30}$ films. The decrease in stiffness and strength was also observed after ion irradiation at room temperature in several Zr-based bulk metallic glasses [**14**,**59**]. Brechtl et *al.* [**60**] found that fast neutron irradiation (E_n>0.1MeV) at 70°C to a fluence of 1.4×10^{20}n/cm^2 induced an excess of free volume defects, which leads to mechanical softening of $Zr_{52.5}Cu_{17.9}Ni_{14.6}Al_{10}Ni_5$ bulk MG and a decrease of Young's modulus. While Onodera et al. [**61**] reported that the drop in hardness is attributed to irradiation-induced atomic disordering in the metallic glass.

The dose-dependence of the change in hardness in metallic glasses is opposite to what is observed in the case of crystalline pure metals and metallic alloy systems [**62**], in which irradiation induces hardening. The evolution of the hardness can be described by the following phenomenological equation [**62**]:

$$\left|\Delta H\right| = \left|(H - H_0)\right| = h(dpa)^n \quad , \tag{2}$$

where h and n are two empirical parameters representing the magnitude of irradiation-softening. H_0 is the hardness of an unirradiated sample and H is the hardness after ion irradiation.

The variation of $\left|\Delta H\right| = \left|(H - H_0)\right|$ as a function of the dose (dpa) is given in Figure 7 in log-log format. It reveals two distinct irradiation regimes: a low-dose regime and a high-dose regime. In the low-dose regime, n is equal to 0.23. However, the slope changes sign beyond a critical dose of about D_c=109 dpa in the high dose-regime. This result reveals that irradiation induces the softening of $Zr_{70}Ni_{30}$ at a dose lower than a critical value of D_c, then the material gradually hardens with increasing dose.

The slight increase of (*H)* and (*E)* values at high fluence (8×10^{13} ions/cm^2) suggests that the thin film reached a saturation in the concentration of defects leading to the high atomic mobility, which subsequently favour rearrangement atomic processes which can then induce nano-crystals formation due to thermal effects. With a further increase in the irradiation fluence, the amount of free volume is reduced, leading to an increase of hardness [**63**]. Other studies [**15**][**64**] deduced the formation of nano-crystals is the fundamental reason for the hardening effect in metallic glasses after ion irradiation. Note that the annealing of Zr bulk MG at 300-325°C leads to free volume annihilation, resulting in structural relaxation and increased mechanical properties. Indeed, structural

relaxation is known to occur through different mechanisms: (i) defects or free volume annihilation; (ii) recombination of defects of opposing character; (iii) change in both topological and compositional short-range order [**65**,**66**]. More research is required to understand the delicate balance of mechanisms that causes the hardness variation at high fluence.

In addition, it should also be noted that the irradiated samples exhibit the same evolution of both (*H)* and (*E)* parameters as was observed earlier in the case of 7 MeV Xe^{26+} ion irradiated $Zr_{50.7}Cu_{28}Ni_9Al_{12.3}$ bulk MG [**28**], where the mechanical properties tend to decrease for a dose of 1 dpa and then to slightly increase at 5 dpa. Our results suggest a strong correlation between hardness and free volume evolution in agreement also with the previous work by Jiang et al. [**67**]. The authors discussed the relationship between the amount of free volume and the mechanical behaviour of metallic glasses.

Finally, Table 2 shows also that the *H*/*E* ratio, a key parameter in the context of wear resistance [**68**], slightly decreases after irradiation up to a fluence of 2×10^{13} ions/cm^2 and then remains almost identical to that of the unirradiated sample at high fluence (>2×10^{13} ions/cm^2). This suggests that ion irradiation does probably not significantly affect the wear resistance of $Zr_{70}Ni_{30}$ metallic glass, which is an interesting finding for application as coating in irradiated environments, especially when explored to moving fluids, such as coating in the nuclear waste containers [**15**,**69**]. New TFMGs with excellent hardness and corrosion resistance were recently developed (see Ref. [**70**] and references therein), making them attractive for coating structural materials. Due to the limited corrosion of zirconium alloys fuel cladding material under accident conditions, oxidation-resistant coatings are used to prevent thermal oxidation and to consequently protect the zirconium alloy substrate [**71**,**72**]. Metallic glass coating based on Zr-composition could constitute an attractive option, with expected good adhesion owing

to element compatibility.

3.3. Thermal spike model calculations

In order to analyze the swift heavy ion irradiation-induced track formation in amorphous $Zr_{70}Ni_{30}$, the thermal spike model, was applied to take into account only the electronic energy loss S_e (keV/ Å) for $^{129}Xe^{23+}$ ion of a specific energy 0.71MeV/u. According to this model, the heat diffusion in the two; electronic (index *e*) and atomic (index *a*) sub-systems is described by the following equations [**36**]:

$$C_e(T_e)\frac{\partial T_e}{\partial t} = \frac{1}{r}\frac{\partial}{\partial r}\left[rK_e(T_e)\frac{\partial T_e}{\partial r}\right] - g(T_e - T_a) + A(r,t) \quad , \tag{3}$$

$$C_a(T_a)\frac{\partial T_a}{\partial t} = \frac{1}{r}\frac{\partial}{\partial r}\left[rK_a(T_a)\frac{\partial T_a}{\partial r}\right] + g(T_e - T_a) \quad , \tag{4}$$

where the parameters T_e, T_a, C_e, C_a, K_e, and K_a are the temperature, the specific heat capacity and the thermal conductivity of the electronic and atomic subsystems, respectively, *g* is the electron-phonon coupling, *t* and *r* are the variables of the time and space from the ion trajectory, and *A(r, t)* is the deposited energy to the target electrons obtained from Monte Carlo simulation in the work of Waligórski et al. [**73**]. The numerical solution of these two equations gives the temperature evolution for the two subsystems as a function of time (*t*) and space (*r*). According to a study conducted by Ichitsubo et al. [**74**], the structure of the $Zr_{70}Ni_{30}$ amorphous alloy resembles that of the Zr_2Ni crystalline phase. So, since there is no literature-available thermodynamic data for $Zr_{70}Ni_{30}$, the calculations were performed using the specific heat of the Zr_2Ni as a function of the temperature from Ref. [**75**].

The thermal conductivity (K) is estimated using the relationship $K=C\ \rho\ D$, where C is the specific heat, ρ is the density, and D= 0.02cm^2 /s is the thermal diffusivity [**76**]. The latent heat of fusion was determined for Zr_2Ni using the software MTDATA and the SGTE solution database. The value for the coupling parameter used for the simulation was taking from reference [**77**].

This calculation gives the variation of atomic temperatures in Kelvin as a function of the time and radius around the ion track, as shown in Figure 8. The horizontal dotted line indicates the melting temperature (T_m). This plot reveals that the lattice temperature reaches the melting point, indicating the phase solid-liquid transformation. This suggests the melting of $Zr_{70}Ni_{30}$ by swift heavy ion irradiation, leading consequently to track ion formation after the quenching of a melting phase. The track radius is about 7 nm, which supports the results obtained by nanoindentation at high fluence. Thus, this simulation indicates that the high deposited energy dissipated in a short time in $Zr_{70}Ni_{30}$ thin film is mainly responsible for induced such point defects and could decrease the free volume leading to increased mechanical properties. However, despite the thermal spike process, structural changes within damage cascades coupled with the free volume and anti-free volume have a significant role in forming nano-crystals after irradiation with 1 MeV Ni^+ ion in the $Ni_{25.5}Nb_{10}Zr_{15}Ti_{15}Pt_{7.5}$ metallic glass ribbon [**78**]. According to the literature, the precipitation of nano-crystals with an average size of 6 nm in the MG under 7MeV Xe^{26+} ion irradiation can also be observed at 5 dpa using the TEM and leading to the increase in the mechanical properties [**28**]. Thus, based on the theoretical analysis results, the track radius with a 7 nm diameter is estimated in our study, but we cannot determine their nature. According to the literature, the TEM analysis visible the nature of the phase formed with their size in the MGs under ion irradiation.

Hence the amorphous metallic glass $Zr_{70}Ni_{30}$ is therefore sensitive to electronic excitations. Thus, depending on the electronic stopping power, latent tracks with spherical and cylindrical morphology can be induced by irradiation in $Zr_{70}Ni_{30}$ metallic glass, which leads to a change in mechanical, electrical and structural properties.

In order to check the electronic energy loss threshold of track formation in the $Zr_{70}Ni_{30}$ metallic glass under $^{126}Xe^{23+}$ ion irradiation, we carried out a series of calculations starting with the Xe ions energy of 0.71MeV/u down to a possible low value using the parameters of the thermal spike model described above. Thus, the track radius formed was estimated for each electronic energy loss at different energies. The results given the evolution of the track radius in $Zr_{70}Ni_{30}$ versus electronic energy loss are shown in Figure 9. The track radius increases above a threshold value of about 6.32 keV/nm. Therefore, the track formation radius starts to be observable in the $Zr_{70}Ni_{30}$ at an electronic energy loss threshold of $S_{eth} \geq$ 6.32 keV/nm.

4. Conclusion

In this investigation, $Zr_{70}Ni_{30}$ thin film metallic glass films deposited onto silicon substrate via the DC magnetron sputtering were irradiated by 0.71MeV/u $^{129}Xe^{23+}$swift heavy ion within the fluence range 5×10^{12} - 8×10^{13} ions/cm^2. The GI-XRD, SEM and AFM analyses revealed that the films are amorphous structure with a thickness of about 1200 nm and the RMS roughness is equal to 0.94 nm. Furthermore, 0.71MeV/u Xe ion irradiation induced surface smoothening and modification of the hardness and Young's modulus. The combination of the AFM and nano-indentation data reveal that at a low irradiation dose up to a critical value of 109 dpa, the irradiation-induced increase of the free volume causes $Zr_{70}Ni_{30}$ softening. An increase of the irradiation dose above 109 dpa presumably leads to the formation of nano-crystals responsible for the slight

increase of the hardness. The nano-crystals are not detected using GI-XRD, and TEM is needed to confirm this claim. Whereas theoretical analysis based on the thermal spike model reveals a track formation with a radius of about 7 nm, to be also confirmed by TEM.

In addition, the electronic energy loss threshold for track generation in $Zr_{70}Ni_{30}$ was calculated to be 6.32 keV/nm using thermal spike calculations.

Acknowledgments

This work was supported by the National Fund for Scientific Research (FNRS), under Grant–T.0178.19 for T. Pardoen, M. Ghidelli. The authors are indebted to GANIL staff for the Xe ions irradiations, Professor Azizi Amor for AFM analysis and Jim A. J. Robinson, for latent heat of fusion calculation.

References

[**1**] P. Hosemann, D. Frazer, M. Fratoni, A. Bolind, M.F. Ashby, Materials selection for nuclear applications: Challenges and opportunities, Scr. Mater. 143 (2018) 181–187. https://doi.org/10.1016/j.scriptamat.2017.04.027.

[**2**] C. Lemaignan, Zirconium Alloys: Properties and Characteristics, in: R.J.M. Konings (Ed.), Compr. Nucl. Mater., Elsevier, Oxford, 2012: pp. 217–232. https://doi.org/10.1016/B978-0-08-056033-5.00015-X.

[**3**] A. Inoue, Stabilization of metallic supercooled liquid and bulk amorphous alloys, Acta Mater. 48 (2000) 279–306. https://doi.org/10.1016/S1359-6454(99)00300-6.

[**4**] A. Inoue, X.M. Wang, W. Zhang, Developments and applications of bulk metallic glasses, Rev. Adv. Mater. Sci. 18 (2008) 1–9.

[**5**] J. Basu, S. Ranganathan, Bulk metallic glasses: A new class of engineering materials, Sadhana - Acad. Proc. Eng. Sci. 28 (2003) 783–798. https://doi.org/10.1007/BF02706459.

[**6**] M.F. Ashby, A.L. Greer, Metallic glasses as structural materials, Scr. Mater. 54

(2006) 321–326. https://doi.org/10.1016/j.scriptamat.2005.09.051.

[**7**] J. Lee, K.H. Huang, K.C. Hsu, H.C. Tung, J.W. Lee, J.G. Duh, Applying composition control to improve the mechanical and thermal properties of Zr-Cu-Ni-Al thin film metallic glass by magnetron DC sputtering, Surf. Coatings Technol. 278 (2015) 132–137. https://doi.org/10.1016/j.surfcoat.2015.07.015.

[**8**] B. Nair, B.G. Priyadarshini, Process, structure, property and applications of metallic glasses, AIMS Mater. Sci. 3 (2016) 1022–1053. https://doi.org/10.3934/matersci.2016.3.1022.

[**9**] G.A. Almyras, G.M. Matenoglou, P. Komninou, C. Kosmidis, P. Patsalas, G.A. Evangelakis, On the deposition mechanisms and the formation of glassy Cu-Zr thin films, J. Appl. Phys. 107 (2010) 084313. https://doi.org/10.1063/1.3366715.

[**10**] M. Ghidelli, S. Gravier, J.J. Blandin, P. Djemia, F. Mompiou, G. Abadias, J.P. Raskin, T. Pardoen, Extrinsic mechanical size effects in thin ZrNi metallic glass films, Acta Mater. 90 (2015) 232–241. https://doi.org/10.1016/j.actamat.2015.02.038.

[**11**] Q.K. Jiang, P. Liu, Y. Ma, Q.P. Cao, X.D. Wang, D.X. Zhang, X.D. Han, Z. Zhang, J.Z. Jiang, Super elastic strain limit in metallic glass films, Sci. Rep. 2 (2012) 3–8. https://doi.org/10.1038/srep00852.

[**12**] D. Jang, J.R. Greer, Transition from a strong-yet-brittle to astronger-and-ductile state by size reductionofmetallicglasses, Nat. Mater. 9 (2010) 215–219. https://doi.org/10.1038/nmat2622.

[**13**] T. Zhang, A. Inoue, T. Masumoto, Amorphous Zr-Al-TM (TM=Co, Ni, Cu) alloys with significant supercooled liquid region of over 100 K, Mater. Trans. JIM. 32 (1991) 1005–1010. https://doi.org/10.2320/matertrans1989.32.1005.

[**14**] A.G. Perez-Bergquist, H. Bei, K.J. Leonard, Y. Zhang, S.J. Zinkle, Effects of ion irradiation on Zr52.5Cu17.9Ni 14.6Al10Ti5 (BAM-11) bulk metallic glass, Intermetallics. 53 (2014) 62–66. https://doi.org/10.1016/j.intermet.2014.04.016.

[**15**] W.D. Luo, B. Yang, G.L. Chen, Effect of Ar+ ion irradiation on the microstructure and properties of Zr-Cu-Fe-Al bulk metallic glass, Scr. Mater. 64 (2011) 625–628. https://doi.org/10.1016/j.scriptamat.2010.12.004.

[**16**] F.J. Li, J.S. Xing, Z.Q. Zhao, B.C. Wei, Damage characteristics of Zr-based

metallic glasses under helium ions irradiation, Mater. Sci. Forum. 849 (2016) 22–27. https://doi.org/10.4028/www.scientific.net/MSF.849.22.

[**17**] B. Wang, X. Mei, H. Zhang, W. Hou, Y. Wang, Z. Wang, C. Dong, Resistance to He2+ induced irradiation damage in metallic glass Zr64Cu17.8Ni10.7Al7.5, J. Nucl. Mater. 444 (2014) 342–348. https://doi.org/10.1016/j.jnucmat.2013.09.058.

[**18**] T. Nagase, T. Hosokawa, Y. Umakoshi, Solid state amorphization and crystallization in Zr66.7Pd33.3 metallic glass, Intermetallics. 14 (2006) 1027–1032. https://doi.org/10.1016/j.intermet.2006.01.021.

[**19**] T. Nagase, M. Nakamura, Y. Umakoshi, Electron irradiation induced nano-crystallization in Zr66.7Ni33.3 amorphous alloy and Zr60Al15Ni25 metallic glass, Intermetallics. 15 (2007) 211–224. https://doi.org/10.1016/j.intermet.2006.05.009.

[**20**] Y. Umakoshi, T. Nagase, T. Hosokawa, Electron irradiation induced crystallization behavior in Zr 66.7M33.3 (M = Cu, Ni, Pd) metallic glasses, Mater. Trans. 48 (2007) 1644–1650. https://doi.org/10.2320/matertrans.MJ200703.

[**21**] H.C. Chen, L. Yan, R.D. Liu, M.B. Tang, G. Wang, H.F. Huang, Y. Hai, X.T. Zhou, Anisotropic nanocrystallization of a Zr-based metallic glass induced by Xe ion irradiation, Intermetallics. 52 (2014) 15–19. https://doi.org/10.1016/j.intermet.2014.03.006.

[**22**] H.C. Chen, G.Q. Cao, R.D. Liu, G. Wang, L. Yan, X.T. Zhou, Ion irradiation induced element-enriched and depleted nanostructures in Zr-Al-Cu-Ni metallic glass, J. Appl. Phys. 118 (2015) 035308. https://doi.org/10.1063/1.4927157.

[**23**] M. Iqbal, J.I. Akhter, Z.Q. Hu, H.F. Zhang, A. Qayyum, W.S. Sun, Mechanical properties and ion irradiation of bulk amorphous Zr55Cu30Al10Ni5 alloy, J. Non. Cryst. Solids. 353 (2007) 2452–2458. https://doi.org/10.1016/j.jnoncrysol.2007.04.013.

[**24**] T. Nagase, T. Sanda, A. Nino, W. Qin, H. Yasuda, H. Mori, Y. Umakoshi, J.A. Szpunar, MeV electron irradiation induced crystallization in metallic glasses: Atomic structure, crystallization mechanism and stability of an amorphous phase under the irradiation, J. Non. Cryst. Solids. 358 (2012) 502–518.

https://doi.org/10.1016/j.jnoncrysol.2011.11.010.

[**25**] J. Brechtl, S. Agarwal, M.L. Crespillo, T. Yang, H. Bei, S.J. Zinkle, Evolution of the microstructural and mechanical properties of BAM-11 bulk metallic glass during ion irradiation and annealing, J. Nucl. Mater. 523 (2019) 299–309. https://doi.org/10.1016/j.jnucmat.2019.06.010.

[**26**] T. Liu, W. Guo, M.L. Crespillo, K. Jin, Y. Zhang, H. Bei, Y. Gao, Indirectly probing the structural change in ion-irradiated Zr-Based metallic glasses from small scale mechanical tests, Intermetallics. 121 (2020) 106794. https://doi.org/10.1016/j.intermet.2020.106794.

[**27**] F. Hori, N. Onodera, Y. Fukumoto, A. Ishii, A. Iwase, A. Kawasuso, A. Yabuuchi, M. Maekawa, Y. Yokoyama, A study of defects in electron- and ion-irradiated ZrCuAl bulk glassy alloy using positron annihilation techniques, J. Phys. Conf. Ser. 262 (2011) 012025. https://doi.org/10.1088/1742-6596/262/1/012025.

[**28**] X.L. Bian, G. Wang, H.C. Chen, L. Yan, J.G. Wang, Q. Wang, P.F. Hu, J.L. Ren, K.C. Chan, N. Zheng, A. Teresiak, Y.L. Gao, Q.J. Zhai, J. Eckert, J. Beadsworth, K.A. Dahmen, P.K. Liaw, Manipulation of free volumes in a metallic glass through Xe-ion irradiation, Acta Mater. 106 (2016) 66–77. https://doi.org/10.1016/j.actamat.2016.01.002.

[**29**] H. Chen, Y. Hai, R. Liu, Q. Lei, L. Ye, J. Xu, G. Wang, W. Yin, L. Yan, X. Zhou, The microstructure and mechanical properties of He+ ion irradiated Zr55Cu30Al10Ni5 bulk metallic glass, Intermetallics. 104 (2019) 52–58. https://doi.org/10.1016/j.intermet.2018.10.022.

[**30**] K. Sun, G. Wang, Y.W. Wang, H.C. Chen, L. Yan, S. Pauly, Y.H. Wu, H. Weber, Q. Wang, B. Huang, Y.D. Jia, J. Yi, Q.J. Zhai, Structural rejuvenation and relaxation of a metallic glass induced by ion irradiation, Scr. Mater. 180 (2020) 34–39. https://doi.org/10.1016/j.scriptamat.2020.01.023.

[**31**] Y.H. Qiu, C. Xu, E.G. Fu, P.P. Wang, J.L. Du, Z.Y. Hu, X.Q. Yan, X.Z. Cao, Y.G. Wang, L. Shao, Mechanisms for the free volume tuning the mechanical properties of metallic glass through ion irradiation, Intermetallics. 101 (2018) 173–178. https://doi.org/10.1016/j.intermet.2018.08.006.

[**32**] R. Frahm, Crystallization behaviour of amorphous nickel-zirconium alloys, J. Non. Cryst. Solids. 56 (1983) 255–260. https://doi.org/10.1016/0022-3093(83)90477-5.

[**33**] K.H.J. Buschow, N.M. Beekmans, Thermal stability and electronic properties of amorphous Zr-Co and Zr-Ni alloys, Phys. Rev. B. 19 (1979) 3843–3849. https://doi.org/10.1103/PhysRevB.19.3843.

[**34**] A.K. Tyagi, R. V. Nandedkar, K. Krishan, Effect of 100 keV helium ion bombardment on surface topography and microstructure of Ni33Zr67 glass, J. Nucl. Mater. 114 (1983) 181–189. https://doi.org/10.1016/0022-3115(83)90255-6.

[**35**] A.K. Tyagi, R. V. Nandedkar, Helium irradiation of Ni-(Zr or Nb) metallic glasses: Blistering, flaking and bubble formation, J. Nucl. Mater. 132 (1985) 62–69. https://doi.org/10.1016/0022-3115(85)90394-0.

[**36**] M. Toulemonde, W. Assmann, C. Dufour, A. Meftah, F. Studer, C. Trautmann, Experimental phenomena and thermal spike description of ion Tracks in Amorphisable Inorganic Insulators, Mat. Fys. Medd. 52 (2006) 263–292.

[**37**] M. Ghidelli, S. Gravier, J.J. Blandin, T. Pardoen, J.P. Raskin, F. Mompiou, Compositional-induced structural change in ZrxNi100-x thin film metallic glasses, J. Alloys Compd. 615 (2014) S348–S351. https://doi.org/10.1016/j.jallcom.2013.12.054.

[**38**] J.F. Ziegler, M.D. Ziegler, J.P. Biersack, SRIM - The stopping and range of ions in matter (2010), Nucl. Instruments Methods Phys. Res. Sect. B Beam Interact. with Mater. Atoms. 268 (2010) 1818–1823. https://doi.org/10.1016/j.nimb.2010.02.091.

[**39**] R.M. Hengstler-Eger, P. Baldo, L. Beck, J. Dorner, K. Ertl, P.B. Hoffmann, C. Hugenschmidt, M.A. Kirk, W. Petry, P. Pikart, A. Rempel, Heavy ion irradiation induced dislocation loops in AREVA's M5® alloy, J. Nucl. Mater. 423 (2012) 170–182. https://doi.org/10.1016/j.jnucmat.2012.01.002.

[**40**] F.M. Mwema, E.T. Akinlabi, O.P. Oladijo, The Use of Power Spectrum Density for Surface Characterization of Thin Films, in: Xiao-Yu Yang (Ed.), Photoenergy Thin Film Mater., John Wiley & Sons, 2019: pp. 379–411.

https://doi.org/10.1002/9781119580546.ch9.

[**41**] I. Horcas, R. Fernández, J. Colchero, J. Gómez-herrero, WSXM : A software for scanning probe microscopy and a tool for nanotechnology, Rev. Sci. Instrum. 78 (2007) 013705. https://doi.org/10.1063/1.2432410.

[**42**] W.C. Oliver, G.M. Pharr, An improved technique for determining hardness and elastic modulus using load and displacement sensing indentation experiments, J. Mater. Res. 7 (1992) 1564–1583. https://doi.org/10.1557/JMR.1992.1564.

[**43**] Y. Yang, J.F. Zeng, A. Volland, J.J. Blandin, S. Gravier, C.T. Liu, Fractal growth of the dense-packing phase in annealed metallic glass imaged by high-resolution atomic force microscopy, Acta Mater. 60 (2012) 5260–5272. https://doi.org/10.1016/j.actamat.2012.06.025.

[**44**] M. Ghidelli, A. Volland, J.J. Blandin, T. Pardoen, J.P. Raskin, F. Mompiou, P. Djemia, S. Gravier, Exploring the mechanical size effects in Zr65Ni35 thin film metallic glasses, J. Alloys Compd. 615 (2015) S90–S92. https://doi.org/10.1016/j.jallcom.2013.11.154.

[**45**] M. Ghidelli, S. Gravier, J.J. Blandin, J.P. Raskin, F. Lani, T. Pardoen, Size-dependent failure mechanisms in ZrNi thin metallic glass films, Scr. Mater. 89 (2014) 9–12. https://doi.org/10.1016/j.scriptamat.2014.06.011.

[**46**] A. Volland, PhD theisis, Etude des effets d'échelle sur le comportement mécanique de film mince en verre métallique, Institut National Polytechnique de Grenoble, 2012.

[**47**] S. Thomas, H. Thomas, D.K. Avasthi, A. Tripathi, R. V. Ramanujan, M.R. Anantharaman, Swift heavy ion induced surface modification for tailoring coercivity in Fe-Ni based amorphous thin films, J. Appl. Phys. 105 (2009) 1–7. https://doi.org/10.1063/1.3075581.

[**48**] H. Thomas, S. Thomas, R. V. Ramanujan, D.K. Avasthi, I.A. Al- Omari, S. Al-Harthi, M.R. Anantharaman, Swift heavy ion induced surface and microstructural evolution in metallic glass thin films, Nucl. Instruments Methods Phys. Res. Sect. B Beam Interact. with Mater. Atoms. 287 (2012) 85–90. https://doi.org/10.1016/j.nimb.2012.05.039.

[**49**] Y. Huang, B. Zhou, H. Fan, Y. Wang, D. Wang, J. Sun, J. Shen, Effect of ion

irradiation in an Al90Fe2Ce8 metallic glass, Mater. Des. 62 (2014) 133–136. https://doi.org/10.1016/j.matdes.2014.05.010.

[**50**] S.G. Mayr, R.S. Averback, Surface smoothing of rough amorphous films by irradiation-induced viscous flow, Phys. Rev. Lett. 87 (2001) 1–4. https://doi.org/10.1103/PhysRevLett.87.196106.

[**51**] W. Hou, X. Mei, X. Zhang, Y. Wang, J. Qiang, J. Sun, Y. Wang, Resistance to He 2+ irradiation damage in metallic glass Ta 38 Ni 62, Appl. Surf. Sci. 383 (2016) 106–112. https://doi.org/10.1016/j.apsusc.2016.05.004.

[**52**] H. Zhang, X. Mei, X. Zhang, X. Li, Y. Wang, J. Sun, Y. Wang, H+-induced irradiation damage resistance in Fe- and Ni-based metallic glass, Nucl. Instruments Methods Phys. Res. Sect. B Beam Interact. with Mater. Atoms. 375 (2016) 79–86. https://doi.org/10.1016/j.nimb.2016.03.015.

[**53**] T. Hysen, P. Geetha, S. Al-Harthi, I.A. Al-Omari, R. Lisha, R. V. Ramanujan, D. Sakthikumar, D.K. Avasthi, M.R. Anantharaman, Effect of 100 MeV Ag+7 ion irradiation on the bulk and surface magnetic properties of Co-Fe-Si thin films, J. Magn. Magn. Mater. 372 (2014) 224–232. https://doi.org/10.1016/j.jmmm.2014.07.005.

[**54**] W.M. Tong, R.S. Williams, Kinetics of surface growth: phenomenology, scaling, and mechanisms of smoothening and roughening, Annu. Rev. Phys. Chem. 45 (1994) 401–438. https://doi.org/10.1146/annurev.pc.45.100194.002153.

[**55**] C. Herring, Effect of change of scale on sintering phenomena, J. Appl. Phys. 21 (1950) 301–303. https://doi.org/10.1063/1.1699658.

[**56**] G. Pookat, T. Hysen, S.H. Al-Harthi, I.A. Al-Omari, R. Lisha, D.K. Avasthi, M.R. Anantharaman, Magnetic and topographical modifications of amorphous Co-Fe thin films induced by high energy Ag7+ ion irradiation, Nucl. Instruments Methods Phys. Res. Sect. B Beam Interact. with Mater. Atoms. 310 (2013) 81–86. https://doi.org/10.1016/j.nimb.2013.05.025.

[**57**] J. Brechtl, H. Wang, N.A.P.K. Kumar, T. Yang, Y.R. Lin, H. Bei, J. Neuefeind, W. Dmowski, S.J. Zinkle, Investigation of the thermal and neutron irradiation response of BAM-11 bulk metallic glass, J. Nucl. Mater. 526 (2019) 151771. https://doi.org/10.1016/j.jnucmat.2019.151771.

[**58**] R. Raghavan, B. Kombaiah, M. Döbeli, R. Erni, U. Ramamurty, J. Michler, Nanoindentation response of an ion irradiated Zr-based bulk metallic glass, Mater. Sci. Eng. A. 532 (2012) 407–413. https://doi.org/10.1016/j.msea.2011.11.004.

[**59**] M. Sadeghilaridjani, A. Ayyagari, S. Muskeri, V. Hasannaeimi, J. Jiang, S. Mukherjee, Small-Scale Mechanical Behavior of Ion-Irradiated Bulk Metallic Glass, Jom. 72 (2020) 123–129. https://doi.org/10.1007/s11837-019-03848-3.

[**60**] J. Brechtl, M.L. Crespillo, S. Agarwal, H. Bei, S.J. Zinkle, Effects of irradiation spectrum on the microstructural and mechanical properties of bulk metallic glasses, J. Nucl. Mater. 533 (2020) 152084. https://doi.org/10.1016/j.jnucmat.2020.152084.

[**61**] N. Onodera, A. Ishii, Y. Fukumoto, A. Iwase, Y. Yokoyama, F. Hori, Local structure and hardness change of Zr 50Cu 40Al 10 bulk glassy alloy after heavy ion irradiation, Nucl. Instruments Methods Phys. Res. Sect. B Beam Interact. with Mater. Atoms. 282 (2012) 1–3. https://doi.org/10.1016/j.nimb.2011.08.049.

[**62**] T.S. Byun, K. Farrell, Irradiation hardening behavior of polycrystalline metals after low temperature irradiation, J. Nucl. Mater. 326 (2004) 86–96. https://doi.org/10.1016/j.jnucmat.2003.12.012.

[**63**] Y. Huang, H. Fan, X. Zhou, P. Xue, Z. Ning, D. Daisenberger, J. Sun, J. Shen, Structure and mechanical property modification of a Ti-based metallic glass by ion irradiation, Scr. Mater. 103 (2015) 41–44. https://doi.org/10.1016/j.scriptamat.2015.03.002.

[**64**] Y.X. Liang, J.L. Du, C. Xu, P.P. Wang, Z.Y. Hu, Y.H. Qiu, P. Wang, E.G. Fu, Roles of ion irradiation and thermal annealing in inducing crystallization in metallic glass, Intermetallics. 114 (2019). https://doi.org/10.1016/j.intermet.2019.106608.

[**65**] H.S. Chen, Structural relaxation in metallic glasses, in: F.E. Luborsky (Ed.), Amorph. Met. Alloy., Butterworth-Heinemann, 1983: pp. 169–186. https://doi.org/10.1016/B978-0-408-11030-3.50016-9.

[**66**] C. Suryanarayana, A. Inoue, Metallic Glasses, in: Ullmann's Encycl. Ind. Chem., Wiley-VCH Verlag GmbH & Co. KGaA, Weinheim, Germany, 2012.

https://doi.org/10.1002/14356007.a16_335.pub2.

[**67**] W.H. Jiang, F.X. Liu, H. Choo, P.K. Liaw, Effect of structural relaxation on mechanical behavior of a Zr-based bulk-metallic glass, Mater. Trans. 48 (2007) 1781–1784. https://doi.org/10.2320/matertrans.MJ200734.

[**68**] A. Leyland, A. Matthews, On the significance of the H/E ratio in wear control: A nanocomposite coating approach to optimised tribological behaviour, Wear. 246 (2000) 1–11. https://doi.org/10.1016/S0043-1648(00)00488-9.

[**69**] L. Shao, B.P. Gorman, A. Aitkaliyeva, N. David Theodore, G. Xie, Nanometer-scale tunnel formation in metallic glass by helium ion irradiation, Appl. Phys. Lett. 101 (2012) 041901. https://doi.org/10.1063/1.4734399.

[**70**] P. Yiu, W. Diyatmika, N. Bönninghoff, Y.C. Lu, B.Z. Lai, J.P. Chu, Thin film metallic glasses: Properties, applications and future, J. Appl. Phys. 127 (2020) 030901. https://doi.org/10.1063/1.5122884.

[**71**] G. Cheol Lee, H. Noh, H. Yeom, H.J. Jo, T. Kyun Kim, M. Kim, K. Sridharan, H. Sun Park, Zirconium-silicide coating on zircaloy-4 substrate for accident tolerance: Effects on oxidation resistance and boiling, Ann. Nucl. Energy. 126 (2019) 350–358. https://doi.org/10.1016/j.anucene.2018.11.019.

[**72**] M.A. Tunes, V.M. Vishnyakov, O. Camara, G. Greaves, P.D. Edmondson, Y. Zhang, S.E. Donnelly, A candidate accident tolerant fuel system based on a highly concentrated alloy thin film, Mater. Today Energy. 12 (2019) 356–362. https://doi.org/10.1016/j.mtener.2019.03.004.

[**73**] M.P.R. Waligórski, R.N. Hamm, R. Katz, The radial distribution of dose around the path of a heavy ion in liquid water, Int. J. Radiat. Appl. Instrumentation. Part D. Nucl. Tracks Radiat. Meas. 11 (1986) 309–319. https://doi.org/10.1016/1359-0189(86)90057-9.

[**74**] T. Ichitsubo, E. Matsubara, J. Saida, H.S. Chen, Local structure and glass transition in Zr-based binary amorphous alloys, Mater. Trans. 46 (2005) 2282–2286. https://doi.org/10.2320/matertrans.46.2282.

[**75**] A. Jana, S. Sridar, S.G. Fries, T. Hammerschmidt, K.C.H. Kumar, Thermodynamic modelling of the Ni – Zr system, Intermetallics. 116 (2020) 106640. https://doi.org/10.1016/j.intermet.2019.106640.

[**76**] M. Yamasaki, S. Kagao, Y. Kawamura, K. Yoshimura, Thermal diffusivity and conductivity of supercooled liquid in Zr41Ti14Cu12Ni10Be23 metallic glass, Appl. Phys. Lett. 84 (2004) 4653–4655. https://doi.org/10.1063/1.1759768.

[**77**] A. Inoue, K. Matsuzaki, T. Masumoto, H.S. Chen, Superconducting and electrical properties of amorphous zirconium-transition metal binary alloys, J. Mater. Sci. 21 (1986) 1258–1268. https://doi.org/10.1007/BF00553260.

[**78**] M. Myers, E.G. Fu, M. Myers, H. Wang, G. Xie, X. Wang, W.K. Chu, L. Shao, An experimental and modeling study on the role of damage cascade formation in nanocrystalization of ion-irradiated Ni52.5Nb10Zr 15Ti15Pt7.5 metallic glass, Scr. Mater. 63 (2010) 1045–1048. https://doi.org/10.1016/j.scriptamat.2010.07.027.

Figures captions

Fig. 1. (a) Grazing incidence X-ray diffraction (GI-XRD) pattern in the range of 20-80°. Dashed line shows the center of the broad halo at 37°, **(b)** Two- and three-dimensional AFM images and **(c)** Cross-sectional FE-SEM micrograph of the as-deposited $Zr_{70}Ni_{30}$ thin-film metallic glass.

Fig. 2. Grazing incidence X-ray diffraction (GI-XRD) patterns of metallic glass $Zr_{70}Ni_{30}$ before after 0.71MeV/u $^{129}Xe^{23+}$ ion irradiation at different fluences. The vertical dotted line indicates the band position. The red line is the Lorentzian fit of the experimental data.

Fig. 3. Two- and three-dimensional AFM images of irradiated $Zr_{70}Ni_{30}$ metallic glass at a fluence of **(a)** 5×10^{12} Xe/cm^2, **(b)** 1×10^{13} Xe/cm^2, **(c)** 2×10^{13} Xe/cm^2, **(d)** 4×10^{13} Xe/cm^2 and **(e)** 8×10^{13} Xe/cm^2.

Fig. 4. Variation of the roughness as a function of the fluence irradiation for $Zr_{70}Ni_{30}$. The dotted line is to guide the eye. The error bars for RMS represent standard deviations obtained from various experimental measurements.

Fig. 5. Power spectral density (PSD) as a function of the spatial frequency of surfaces for $Zr_{70}Ni_{30}$ before and after ion irradiation.

Fig. 6. Variation of nano-hardness (H) and Young's modulus (E) of metallic glass $Zr_{70}Ni_{30}$ as a function of fluences irradiation, with the statistical standard deviations obtained from repeated experimental measurements.

Fig. 7. Dose dependence of irradiation softening / hardening in $Zr_{70}Ni_{30}$. The solid line is the linear fit of the experimental data. The dotted line indicates the dose-dependence at a high dose regime.

Fig. 8. Variation of the atomic temperature for $Zr_{70}Ni_{30}$ as a function of the time at different track radii caused by 0.71MeV/u $^{129}Xe^{23+}$ ions irradiation. The dotted line indicates the melting temperature T_m.

Fig. 9. Variation of the track radius as a function of the electronic energy loss in $Zr_{70}Ni_{30}$ thin film for different deposited energies by $^{129}Xe^{23+}$ ion irradiation. The line in the plot is the fit of the data points.

Table 1

Mechanical properties of the $Zr_{70}Ni_{30}$ thin film before and after ion irradiation from the nanoindentation experiments.

Table 2

Root mean square (RMS) roughness and calculated values of the slope of the power spectral density (PSD) curves of unirradiated and irradiated $Zr_{70}Ni_{30}$ thin film at different fluences.

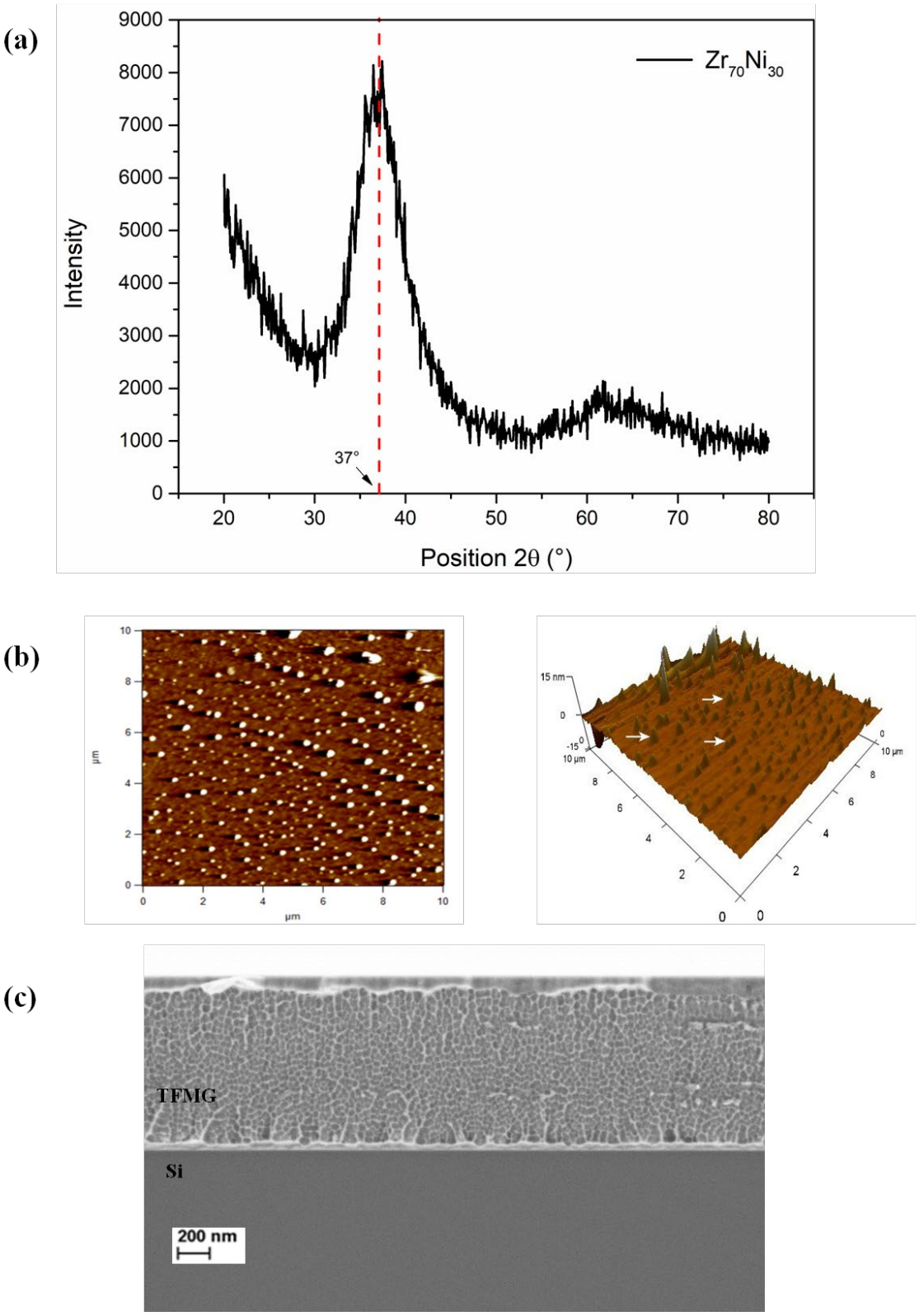
(a)
Intensity
Position 2θ (°)
$Zr_{70}Ni_{30}$
37°
(b)
μm
15 nm
10 μm
(c)
TFMG
Si
200 nm

Fig. 1.

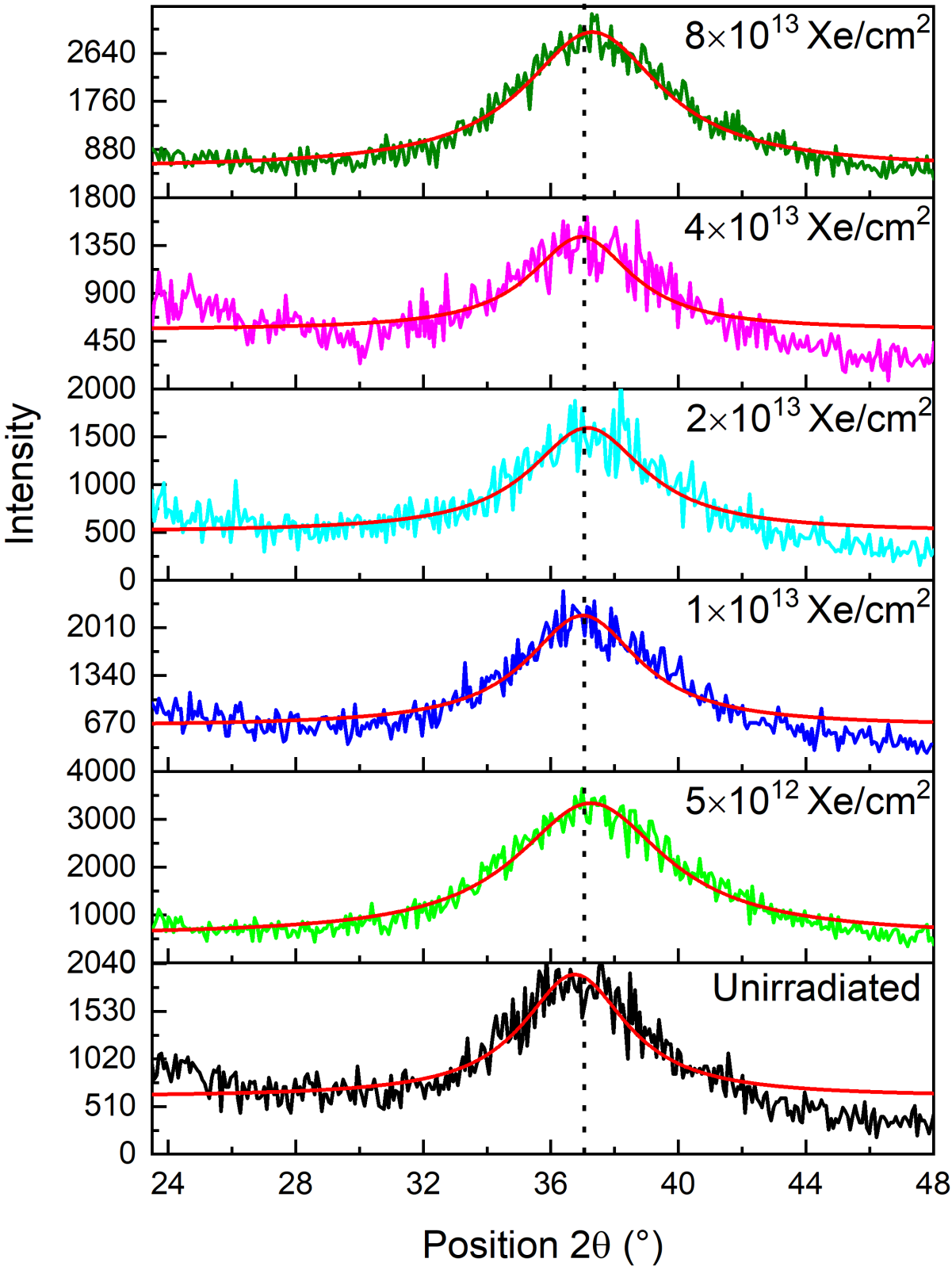
8×10^13 Xe/cm^2
4×10^13 Xe/cm^2
2×10^13 Xe/cm^2
1×10^13 Xe/cm^2
5×10^12 Xe/cm^2
Unirradiated
Intensity
Position 2θ (°)
2640
1760
880
1800
1350
900
450
2000
1500
1000
500
0
2010
1340
670
4000
3000
2000
1000
2040
1530
1020
510
0
24
28
32
36
40
44
48

Fig. 2.

(a). 5×10^{12} ions/cm^2

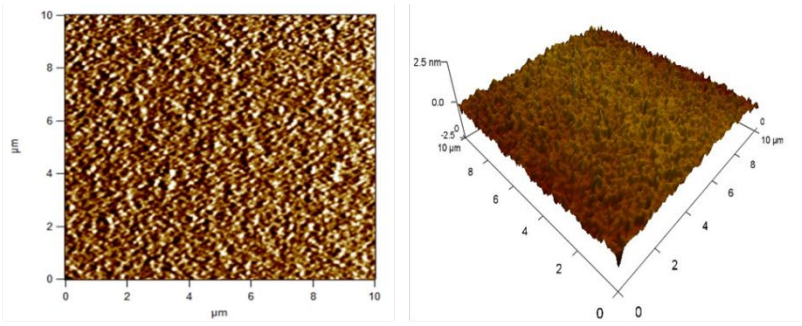

(b). 1×10^{13} ions/cm^2

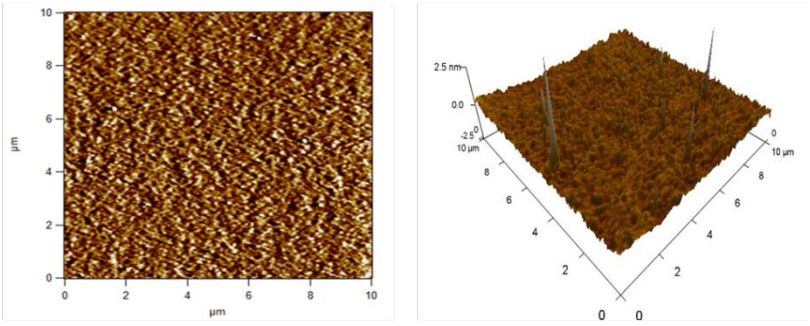

(c). 2×10^{13} ions/cm^2

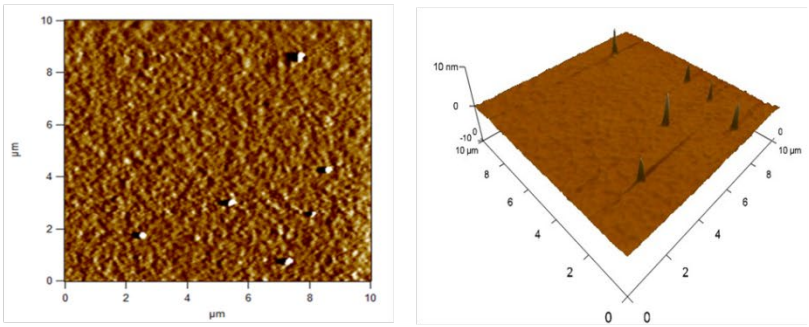

(d). 4×10^{13} ions/cm^2

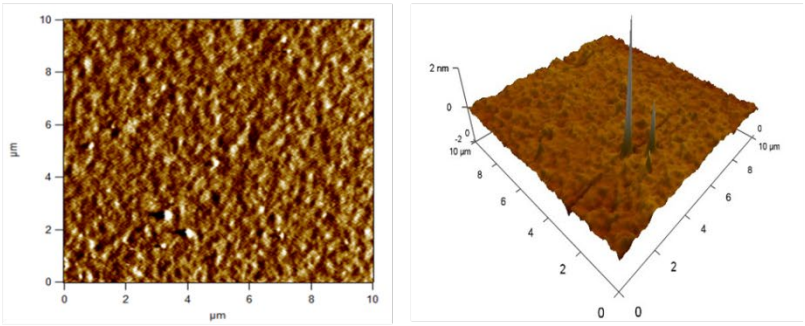

(e). 8×10^{13} ions/cm^2

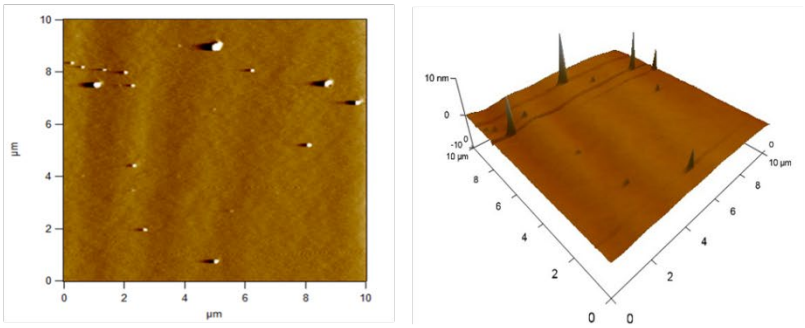

Fig. 3.

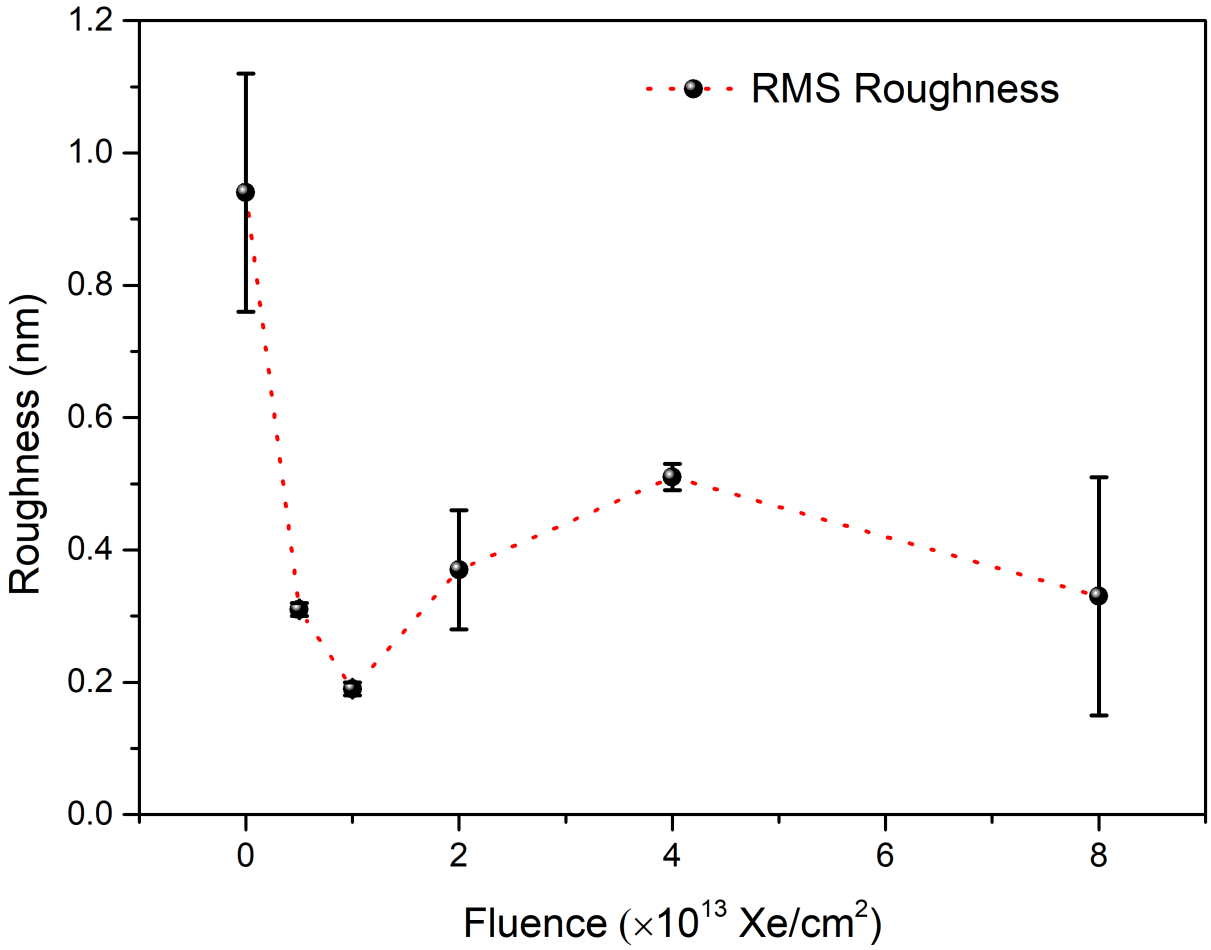
RMS Roughness
Roughness (nm)
1.2
1.0
0.8
0.6
0.4
0.2
0.0
0
2
4
6
8
Fluence (×10^13 Xe/cm^2)

Fig. 4.

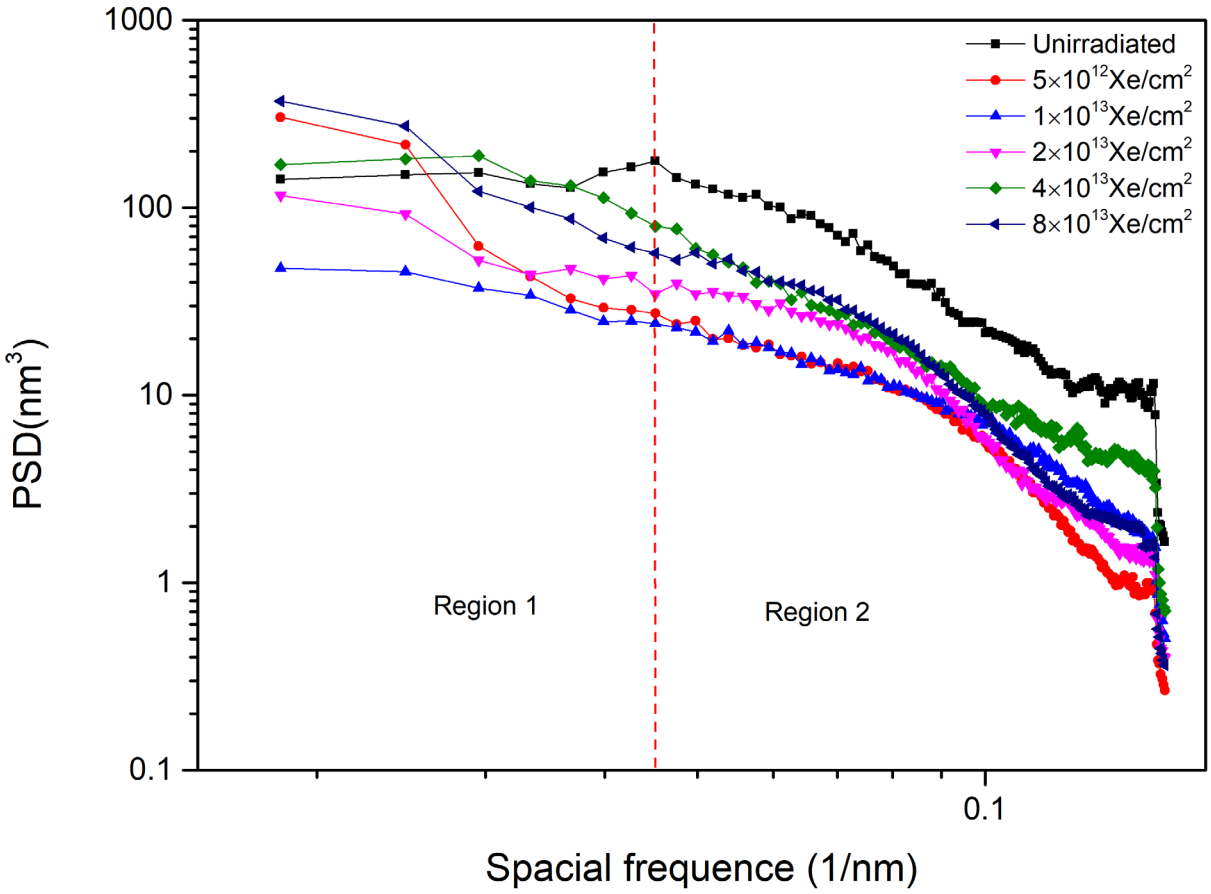
1000
100
10
1
0.1
PSD(nm3)
Region 1
Region 2
0.1
Spacial frequence (1/nm)
Unirradiated
5×10^12Xe/cm^2
1×10^13Xe/cm^2
2×10^13Xe/cm^2
4×10^13Xe/cm^2
8×10^13Xe/cm^2

Fig. 5.

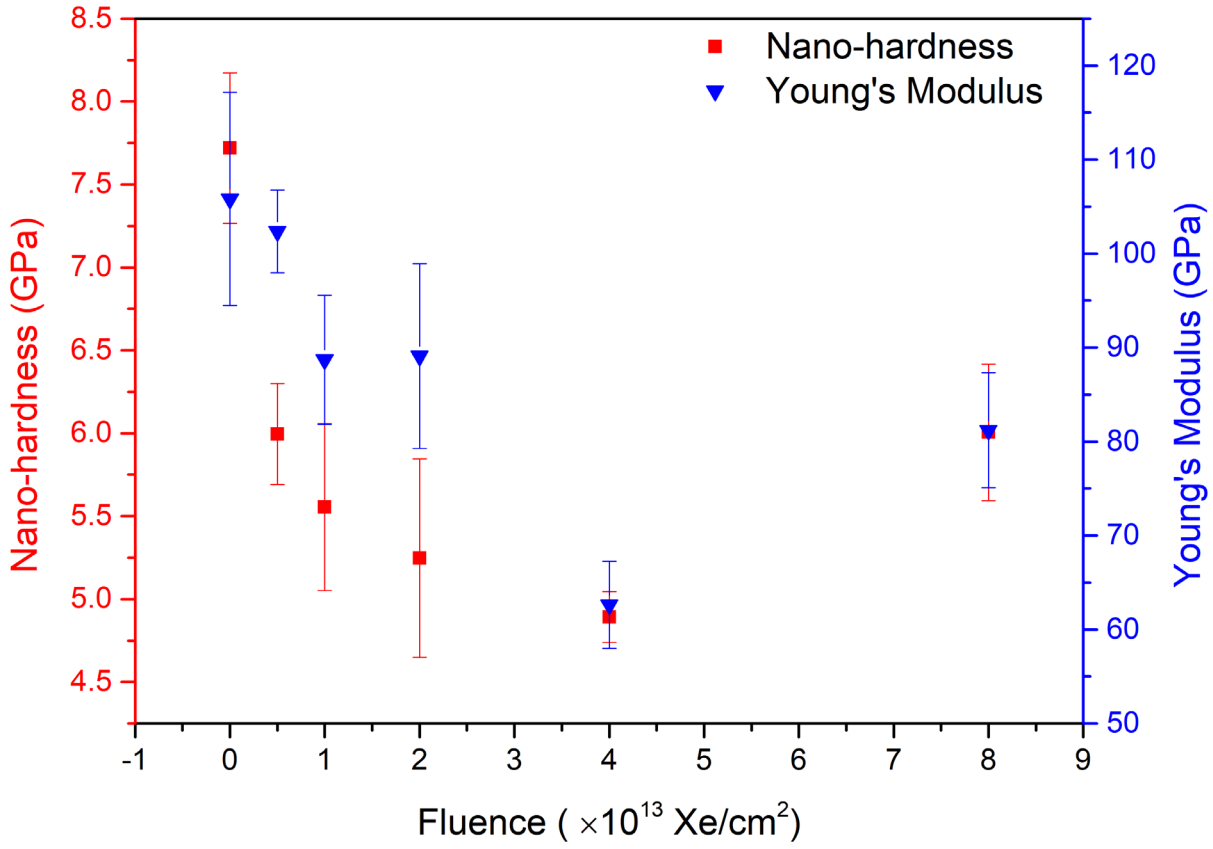
Nano-hardness
Young's Modulus
Nano-hardness (GPa)
Young's Modulus (GPa)
Fluence (×10^13 Xe/cm^2)
8.5
8.0
7.5
7.0
6.5
6.0
5.5
5.0
4.5
120
110
100
90
80
70
60
50
-1
0
1
2
3
4
5
6
7
8
9

Fig. 6.

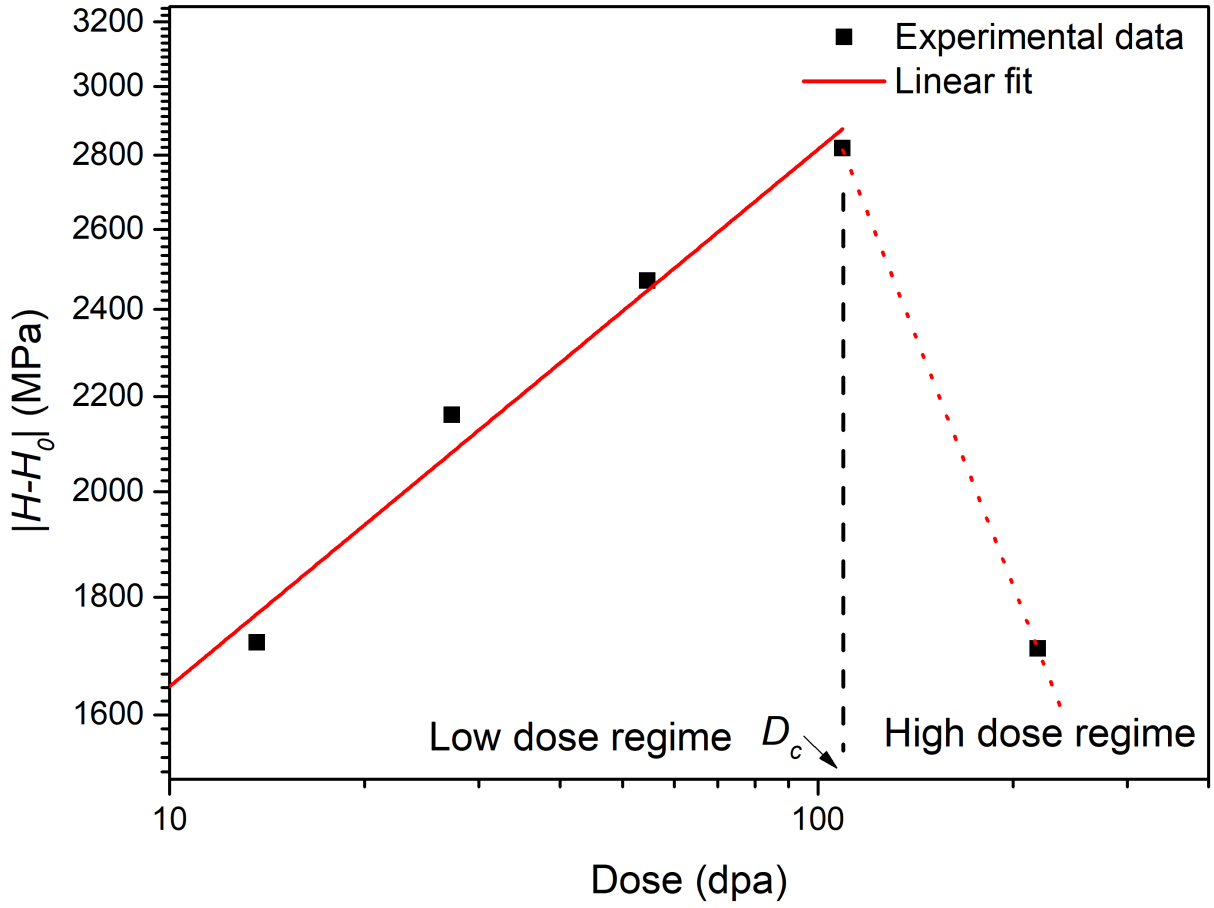
Experimental data
Linear fit
3200
3000
2800
2600
2400
2200
2000
1800
1600
|H-H0| (MPa)
Low dose regime
Dc
High dose regime
10
100
Dose (dpa)

Fig. 7.

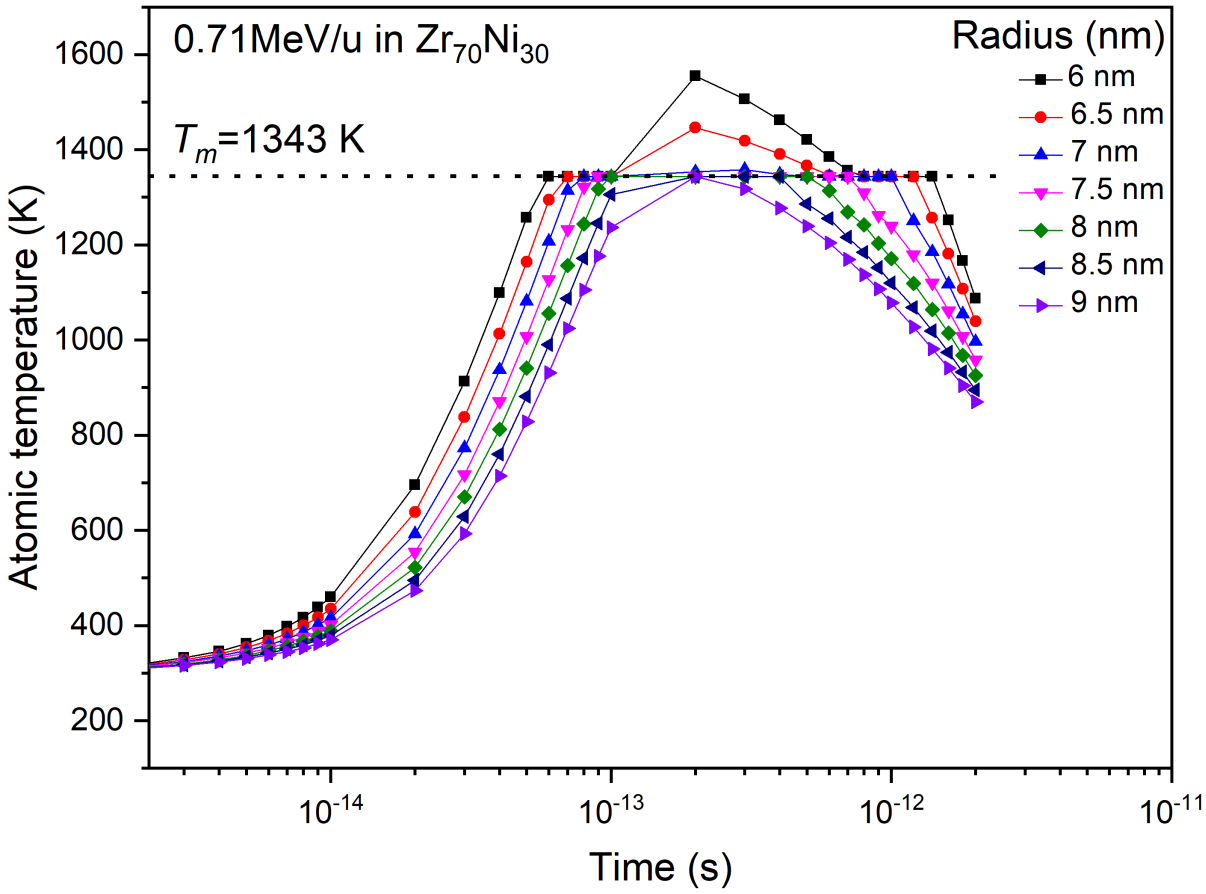
0.71MeV/u in $Zr_{70}Ni_{30}$
T_m=1343 K
Radius (nm)
6 nm
6.5 nm
7 nm
7.5 nm
8 nm
8.5 nm
9 nm
Atomic temperature (K)
1600
1400
1200
1000
800
600
400
200
10^{-14}
10^{-13}
10^{-12}
10^{-11}
Time (s)

Fig. 8.

.

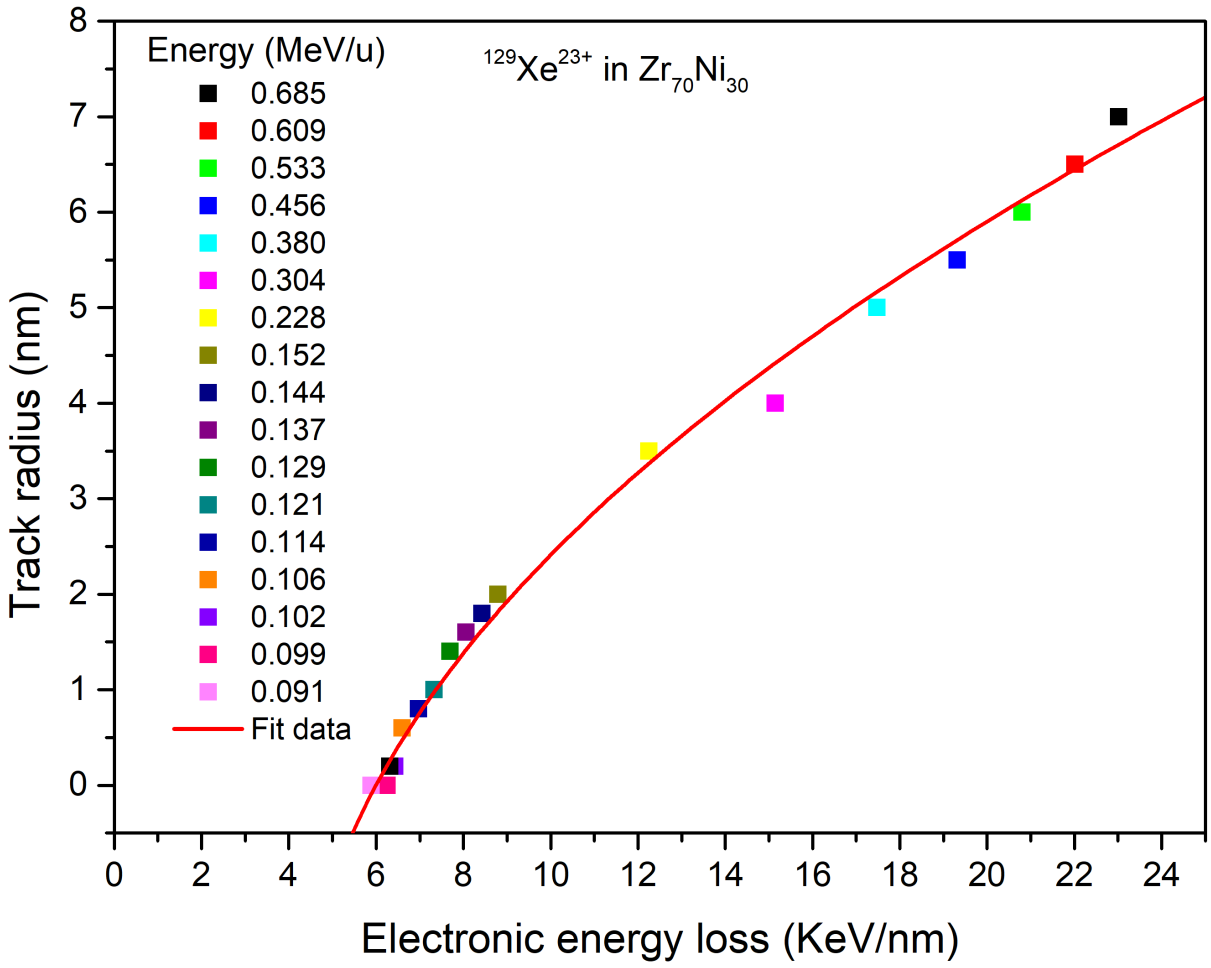
Energy (MeV/u)
0.685
0.609
0.533
0.456
0.380
0.304
0.228
0.152
0.144
0.137
0.129
0.121
0.114
0.106
0.102
0.099
0.091
Fit data
$^{129}Xe^{23+}$ in $Zr_{70}Ni_{30}$
Track radius (nm)
Electronic energy loss (KeV/nm)
0
1
2
3
4
5
6
7
8
0
2
4
6
8
10
12
14
16
18
20
22
24

Fig. 9.

Irradiation fluence (Xe/cm^2)	RMS (nm)	slope of the PSD curve
0	0.94±0.18	2.84±0.04
5×10^{12}	0.31±0.01	1.86±0.06
1×10^{13}	0.19±0.01	1.67±0.03
2×10^{13}	0.37±0.09	1.87±0.10
4×10^{13}	0.51±0.02	2.64±0.04
8×10^{13}	0.33±0.18	2.07±0.09

Table 1

Irradiation fluence (Xe/cm^2)	Nano-hardness H (GPa)	Young's Modulus E (GPa)	H/E
0	7.72±0.45	105.79±11.34	0.07±0.01
5×10^{12}	5.99±0.30	102.35±4.39	0.06±0.01
1×10^{13}	5.55±0.50	88.71±6.86	0.06±0.01
2×10^{13}	5.24±0.60	89.09±9.82	0.06±0.01
4×10^{13}	4.89±0.15	62.63±4.64	0.08±0.01
8×10^{13}	6.00±0.41	81.19±6.10	0.07±0.01

Table 2